Proceedings of the 20th National Conference on Superconductivity "New Phases, Concepts and Advances"

Superconducting Energy Gap in Hole-Doped Graphene Beyond the Migdal's Theory

A.Z. Kaczmarek[a,*] and E.A. Drzazga-Szczęśniak[b]

[a] *Department of Theoretical Physics, Faculty of Science and Technology, Jan Długosz University in Częstochowa, 13/15 Armii Krajowej Ave., 42200 Częstochowa, Poland*
[b] *Department of Physics, Faculty of Production Engineering and Materials Technology, Częstochowa University of Technology, 19 Armii Krajowej Ave., 42200 Częstochowa, Poland*

Doi: 10.12693/APhysPolA.143.153 *e-mail: adam.kaczmarek@doktorant.ujd.edu.pl

In this work, we analyze the impact of non-adiabatic effects on the superconducting energy gap in hole-doped graphene. By using the Eliashberg formalism beyond Migdal's theorem, we present that non-adiabatic effects strongly influence the superconducting energy gap in the exemplary boron-doped graphene. In particular, non-adiabatic effects, as represented by the first-order vertex corrections to the electron–phonon interaction, supplement the Coulomb depairing correlations and suppress the superconducting state. In summary, the obtained results confirm previous studies on superconductivity in two-dimensional materials and show that the corresponding superconducting phase may be notably affected by non-adiabatic effects.

topics: superconducting, hole-doped graphene, Eliashberg formalism

1. Introduction

The discovery of graphene has led to the ever-growing interest in its electronic properties [1]. Among the various electronic aspects, notable attention was given to the induction of the conventional superconducting state in this material. In this respect, one of the most promising scenarios were realized via doping graphene with foreign atoms [2–5]. In general, there are two main routes to enhance the graphene's electron–phonon coupling (λ). The first is the so-called surface functionalization, where metal atoms are deposited on the surface of the monolayer [2, 6, 7]. Unfortunately, in this approach, the resulting critical temperature of the superconductive state (T_C) is rather low. However, the second strategy aims at introducing impurities that act like electron or hole dopants and lead to much higher T_C values [3, 4, 8].

Along with relatively high T_C values of substitutionally doped graphene, such material exhibits a shallow conduction band [3, 4], similarly to fullerenes and fullerides [9–12]. This leads to a significant value of the ratio of the phonon to electron energy scales ($\omega_{\mathrm{D}}/E_{\mathrm{F}}$, where ω_{D} is the Debye's frequency and E_{F} denotes Fermi energy), which cannot be neglected in the framework of Migdal's theorem [13]. Such behavior results in non-adiabatic effects strongly influencing the superconducting phase [14, 15]. As suggested in [14, 16], non-adiabatic effects may have nontrivial impact on the electron–phonon interaction, as can be observed from the behavior of the order parameter. For example, the proper characterization of these effects in graphene has recently been described for the electron-doped graphene structures in [8]. To be specific, the authors of [8] showed that the contribution of non-adiabatic effects rises upon the increase of the Coulomb interaction.

With respect to the above, we investigate non-adiabatic effects in the case of hole-doped graphene to determine their impact on the order parameter and the T_C value. To do so, we employ the Eliashberg equations [17] with the first order vertex-corrections [11, 15, 18]. Calculations are made for the 50% boron-doped graphene structure (h-CB) under biaxial tensile strain $\epsilon = 5\%$ and at a moderate level of dopant electrons ($n = -0.2|e|$/unit cell) [4].

2. Theoretical model

As already mentioned, the present analysis is based on the Eliashberg formalism [17, 19]. Conventionally, this formalism is employed within the adiabatic regime, i.e., by assuming Migdal's theorem [13]. However, to analyze the non-adiabatic effect the Eliashberg equations are additionally generalized here by considering the first-order vertex corrections to the electron–phonon interaction [14, 18, 20].

Specifically, we assume that the adiabatic Eliashberg equations on the imaginary axis have the form

$$\phi_n = \pi k_{\mathrm{B}} T \sum_{m=-M}^{M} \frac{\left[K_{n,m} - \mu^\star\,\theta(\omega_c - |\omega_m|)\right]}{\sqrt{\omega_m^2 Z_m^2 + \phi_m^2}}\,\phi_m, \tag{1}$$

$$Z_n = 1 + \pi k_{\mathrm{B}} T \sum_{m=-M}^{M} \frac{K_{n,m}}{\sqrt{\Delta_m^2 + \omega_m^2}}\,\frac{\omega_m}{\omega_n}\,Z_m. \tag{2}$$

where $\phi_n = \phi(\mathrm{i}\omega_n)$ denotes the order parameter function and $Z_n = Z(\mathrm{i}\omega_n)$ is the renormalization factor of the wave function. In what follows, k_{B} is Boltzmann's constant, T denotes temperature, and ω_n represents the n-th Matsubara frequency ($\omega_n = \pi k_{\mathrm{B}} T(2n+1)$). In this framework, M is the cut-off value for calculations and is equal to 1100, so the numerical calculations are stable for $T > 5$ K. Moreover, $\mu_n^\star = \mu^\star\,\theta(\omega_c - |\omega_n|)$ is the Coulomb pseudopotential that models the depairing correlations, where θ is the Heaviside function and ω_c represents the cut-off frequency.

In the above equations, the electron–phonon pairing kernel is expressed as

$$K_{n,m} \equiv 2\int_0^{\omega_{\mathrm{D}}} \frac{\mathrm{d}\omega\,\omega}{4\pi^2 k_{\mathrm{B}}^2 T^2 (n-m)^2 + \omega^2}\,\alpha^2 F(\omega), \tag{3}$$

where $\alpha^2 F(\omega)$ denotes the Eliashberg function for a given ω phonon energy

$$\alpha^2 F(\omega) = \frac{1}{2\pi\rho\,(E_{\mathrm{F}})} \sum_{\boldsymbol{q}\nu} \delta(\omega - \omega_{\boldsymbol{q}\nu})\,\frac{\gamma_{\boldsymbol{q}\nu}}{\omega_{\boldsymbol{q}\nu}}, \tag{4}$$

whereas

$$\gamma_{\boldsymbol{q}\nu} = 2\pi\omega_{\boldsymbol{q}\nu} \sum_{ij} \int \frac{\mathrm{d}^3 k}{\Omega_{\mathrm{BZ}}} \left|g_{\boldsymbol{q}\nu}(\boldsymbol{k}, i, j)\right|^2 \times \delta(E_{\boldsymbol{q},i} - E_{\mathrm{F}})\,\delta(E_{\boldsymbol{k}+\boldsymbol{q},j} - E_{\mathrm{F}}). \tag{5}$$

In (5), $\omega_{\boldsymbol{q}\nu}$ gives the phonon energies values and $\gamma_{\boldsymbol{q}\nu}$ denotes the phonon linewidth. In this context, the electron–phonon coefficients are represented by $g_{\boldsymbol{q}\nu}(\boldsymbol{k}, i, j)$ and $E_{\boldsymbol{k},i}$ stands for the electron band energy. Note that higher order corrections are not included in (3) and that the momentum dependence of the electron–phonon matrix elements has been neglected in (6) and (7) (according to the local approximation). Therefore, the order parameter can be written as $\Delta_n(T, \mu^\star) = \phi_n / Z_n$. Finally, note that for the purpose of our research, we use the Eliashberg function given in [4]. It is important to remark, that the resulting cutoff frequency in (1) is $\omega_C = 10\omega_{\max}$ with the maximum phonon frequency equal to $\omega_{\max} = 124.47$ meV.

With respect to the presented adiabatic equations, the introduction of the first-order vertex correction terms leads to the non-adiabatic Eliashberg equations (N-E) of the following form [8, 20]

$$\phi_n = \pi k_{\mathrm{B}} T \sum_{m=-M}^{M} \frac{K_{n,m} - \mu_m^\star}{\sqrt{\omega_m^2 Z_m^2 + \phi_m^2}}\,\phi_m - \beta\,\frac{\pi^3\,(k_{\mathrm{B}} T)^2}{4E_{\mathrm{F}}} \times \sum_{m=-M}^{M}\sum_{m'=-M}^{M} \frac{K_{n,m}K_{n,m'}}{\sqrt{\left(\omega_m^2 Z_m^2 + \phi_m^2\right)\left(\omega_{m'}^2 Z_{m'}^2 + \phi_{m'}^2\right)\left(\omega_{-n+m+m'}^2 Z_{-n+m+m'}^2 + \phi_{-n+m+m'}^2\right)}} \times \Big(\phi_m\phi_{m'}\phi_{-n+m+m'} + 2\phi_m\omega_{m'}Z_{m'}\omega_{-n+m+m'}Z_{-n+m+m'} - \omega_m Z_m \omega_{m'} Z_{m'}\phi_{-n+m+m'}\Big), \tag{6}$$

and

$$Z_n = 1 + \frac{\pi k_{\mathrm{B}} T}{\omega_n} \sum_{m=-M}^{M} \frac{K_{n,m}}{\sqrt{\omega_m^2 Z_m^2 + \phi_m^2}}\,\omega_m Z_m - \beta\frac{\pi^3\,(k_{\mathrm{B}} T)^2}{4E_{\mathrm{F}}\,\omega_n} \times \sum_{m=-M}^{M}\sum_{m'=-M}^{M} \frac{K_{n,m}K_{n,m'}}{\sqrt{\left(\omega_m^2 Z_m^2 + \phi_m^2\right)\left(\omega_{m'}^2 Z_{m'}^2 + \phi_{m'}^2\right)\left(\omega_{-n+m+m'}^2 Z_{-n+m+m'}^2 + \phi_{-n+m+m'}^2\right)}} \times \Big(\omega_m Z_m \omega_{m'} Z_{m'}\omega_{-n+m+m'}Z_{-n+m+m'} + 2\omega_m Z_m \phi_{m'}\phi_{-n+m+m'} - \phi_m\phi_{m'}\omega_{-n+m+m'}Z_{-n+m+m'}\Big). \tag{7}$$

Note that when the vertex-corrections contribution terms are neglected, the above Eliashberg equations take the adiabatic form of (1) and (2).

3. Results and discussion

We begin our discussion by noting that the adiabatic (A-E) and the non-adiabatic (N-E) equations presented in the previous section allow us to obtain the order parameter dependence on temperature in the form $\Delta_n(T, \mu^\star) = \phi_n / Z_n$. This is done by using numerical techniques presented originally in [20–22]. In such an analysis, special attention is paid to the maximum value of the order parameter $\Delta_{m=1}(T, \mu^\star)$, which is equal to zero when $T = T_C$ and $\mu^\star = \mu_C^\star$. In other words, it allows us to determine the critical value of temperature for a given critical value of the Coulomb pseudopotential ($\mu_C^\star$),

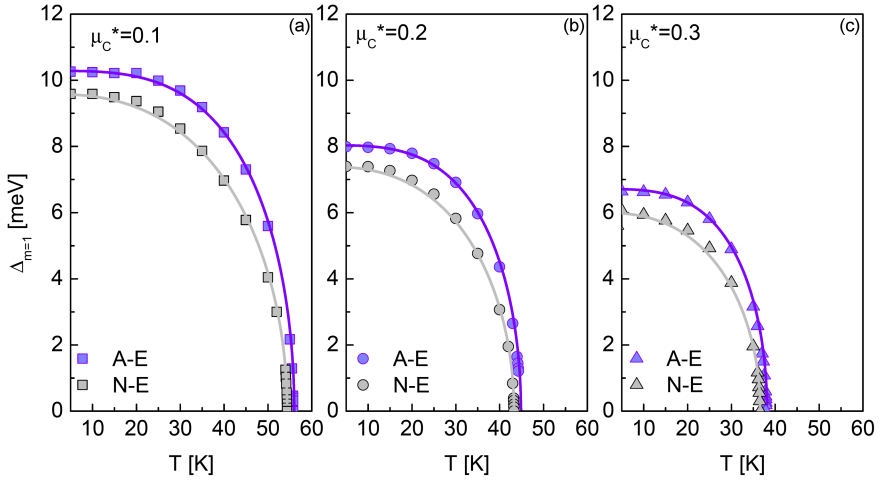

Fig. 1. The temperature dependence of the order parameter for selected μ values. The adiabatic Eliashberg solutions are marked by purple symbols whereas the non-adiabatic results by gray ones. Solid lines are guides to an eye.

which is considered here as a free parameter. The latter was assumed due to the fact that in the literature there are no experimental predictions of T_C for hole-doped graphene.

Specifically, our analysis is constrained to three different values of $\mu_C^\star$. In this way, we can span a relatively wide range of the $\mu^\star$ values, allowing future comparisons with the existing literature on graphene-based superconductors [22–24] or with experimental estimates. Figure 1 depicts the results of the numerical analysis for three different values of $\mu^\star$. Adiabatic solutions are represented by purple symbols, while gray symbols correspond to non-adiabatic Eliashberg equations associated with vertex corrections. The presented results exhibit the conventional behavior for superconductors with electron–phonon pairing mechanism, where $\Delta_{m=1}$ has plateau at lower temperatures and decreases quickly for higher temperatures.

However, the main observation can be made when comparing adiabatic and non-adiabatic results. Namely, the inclusion of vertex corrections in the theoretical framework leads to the decrease of the $\Delta_{m=1}$ parameter for the entire range of T and $\mu^\star$. Thermodynamic properties originating from this fact may be observed in the experiment. To be specific, lower $\Delta_{m=1}$ for non-adiabatic equations leads to $T_C \in \langle 54.4, 36.6\rangle$ K compared to the values obtained for the adiabatic scenario $T_C \in \langle 55.8, 37.9\rangle$ K. Therefore, non-adiabatic effects slightly lower the critical temperature by $\sim 1\%$. We note that upon comparison with electron-doped graphene [8], the decrease of T_C is smaller. For the h-CN structure, changes are actually noticeable. To be specific, in the non-adiabatic framework, the critical temperature decreases by about 30%. Henceforth, non-adiabatic effects in hole-doped graphene are more favorable from the standpoint of keeping the nominal T_C as high as possible. The influence of non-adiabatic effects is another suppressor of high T_C values next to the Coulomb pseudopotential. The implications of non-adiabatic effects can also be seen at the origin of the temperature axis. In particular, $\Delta_{m=1}$ for T_0, which corresponds to the half-width of the superconducting gap (Δ), is also lower for non-adiabatic solutions than in the adiabatic case. Upon the increase of $\mu^\star$, $\Delta \in \langle 10.3, 6.7\rangle$ meV for the adiabatic case and $\Delta \in \langle 9.6, 6.0\rangle$ meV for the non-adiabatic case. Hence, the inclusion of the vertex corrections decreases the values of Δ by $\sim 5\%$ and $\sim 10\%$, respectively. By comparison with the twin h-CN material, the results of these corrections are significantly smaller [8]. In fact, non-adiabatic effects in the electron-doped graphene reduce the value of the order parameter by about 40%.

From the perspective of future experimental search, the obtained values of Δ and T_C parameters may not insufficient for the identification of non-adiabatic effects in hole-doped graphene. Thus, one should calculate the characteristic ratio for the order parameter [19]

$$R_\Delta \equiv \frac{2\Delta(0)}{k_{\mathrm{B}} T_C}. \tag{8}$$

In fact, (8) originates from the BCS theory [25, 26] and as a dimensionless parameter it is important from the perspective of experiments conducted in the future. Here, using (8) we obtain $R_\Delta \in \langle 4.08, 3.79\rangle$ and $R_\Delta \in \langle 4.28, 4.09\rangle$. Again, non-adiabatic effects lead to the reduction of the thermodynamic parameter value. It is important to note that for both types of the Eliashberg equations, the R_Δ parameter values are higher than the standard BCS value of 3.53 [19, 25, 26]. Moreover, the difference between the non-adiabatic and adiabatic values of the characteristic ratio R_Δ is much smaller than the ratio encountered in the case of its nitrogen-doped counterpart [8]. From the analysis

TABLE I

The thermodynamic quantities of hole-doped graphene calculated in the present paper: critical temperature T_C, superconducting gap half-width (Δ), and characteristic ratio R_Δ. Results are obtained for the adiabatic (A-E) and non-adiabatic (N-E) Eliashberg approach.

$\mu^\star$	T_C (A-E) [K]	T_C (N-E) [K]	Δ (A-E) [meV]	Δ (N-E) [meV]	R_Δ (A-E)	R_Δ (N-E)
0.1	55.8	54.4	10.3	9.6	4.27	4.08
0.2	44.1	43.1	8.1	7.3	4.16	3.96
0.3	37.9	36.6	6.7	6.0	4.09	3.79

presented above, one can also conclude that the retardation effects and strong coupling affect superconducting state in hole-doped graphene.

4. Conclusions

We have tackled theoretical and numerical analysis within the Eliashberg theory to discuss the possible impact of non-adiabatic effects on the thermodynamic properties of the superconducting state in hole-doped graphene (h-CB). Our analysis has been performed to analyze the behavior of the critical temperature (T_C), the superconducting gap half-width (Δ), and the dimensionless BCS-ratio for the order parameter (R_Δ). The values of these parameters for adiabatic and non-adiabatic equations are summarized and presented in Table I. Is it clear that the inclusion of non-adiabatic effects via vertex corrections to the electron–phonon interaction reduces the values of the thermodynamic parameters. It is also worth noticing that for the stronger electron-coupling, displayed by higher values of $\mu^\star$, the non-adiabatic effects become slightly stronger. In other words, the Coulomb interaction is supplemented by non-adiabatic effects. Moreover, these effects are significantly smaller than in the case of the electron-doped graphene analyzed in [8]. This means that hole-doped graphene is more robust against non-adiabatic effects since these effects minimally lower its critical temperature (T_C).

Finally, the results presented here supplement the observations conducted for the electron-doped graphene structure [8]. Compared to the electron-doping, the hole-doped structure is more robust against the non-adiabatic effects [8]. However, the superconducting properties will still be reduced in the framework of the vertex-corrected Eliashberg equations. In general, hole-doped graphene may be a still interesting choice for phonon-induced superconducting material.

References

[1] A.H. Castro Neto, F. Guinea, N.M.R. Peres, K.S. Novoselov, A.K. Geim, *Rev. Mod. Phys.* **81**, 109 (2009).

[2] G. Profeta, M. Calandra, F. Mauri, *Nat. Phys.* **8**, 131 (2012).

[3] G. Savini, A.C. Ferrari, F. Giustino, *Phys. Rev. Lett.* **105**, 037002 (2010).

[4] J. Zhou, Q. Sun, Q. Wang, P. Jena, *Phys. Rev. B* **92**, 064505 (2015).

[5] R. Gholami, R. Moradian, S. Moradian, W.E. Pickett, *Sci. Rep.* **8**, 13795 (2018).

[6] J. McChesney, A. Bostwick, T. Ohta, T. Seyller, K. Horn, J. González, E. Rotenberg, *Phys. Rev. Lett.* **104**, 136803 (2010).

[7] J. Zhou, Q. Sun, Q. Wang, P. Jena, *Phys. Rev. B* **90**, 205427 (2014).

[8] D. Szczęśniak, E.A. Drzazga-Szczęśniak, *Eur. Phys. Lett.* **135**, 67002 (2021).

[9] M.P.M. Dean, C.A. Howard, S.S. Saxena, M. Ellerby, *Phys. Rev. B* **81**, 045405 (2010).

[10] Y. Cao, V. Fatemi, S. Fang, K. Watanabe, T. Taniguchi, E. Kaxiras, P. Jarillo-Herrero, *Nature* **556**, 43 (2018).

[11] L. Pietronero, *Eur. Phys. Lett.* **17**, 365 (1992).

[12] O. Gunnarsson, *Rev. Mod. Phys.* **69**, 575 (1997).

[13] A.B. Migdal, *Sov. Phys. JETP* **34**, 996 (1958).

[14] L. Pietronero, S. Strässler, C. Grimaldi, *Phys. Rev. B* **52**, 10516 (1995).

[15] C. Grimaldi, L. Pietronero, S. Strässler, *Phys. Rev. B* **52**, 10530 (1995).

[16] L. Pietronero, E. Cappelluti, *Low Temp. Phys.* **32**, 340 (2006).

[17] G.M. Eliashberg, *Sov. Phys. JETP* **11**, 696 (1960).

[18] L. Pietronero, S. Strässler, *Eur. Phys. Lett.* **18**, 627 (1992).

[19] J.P. Carbotte, *Rev. Mod. Phys.* **62**, 1027 (1990).

[20] J. K. Freericks, E.J. Nicol, A.Y. Liu, A.A. Quong, *Phys. Rev. B* **55**, 11651 (1997).

[21] R. Szczęśniak, *Acta Phys. Pol. A* **109**, 179 (2006).

[22] D. Szczęśniak, R. Szczęśniak, *Phys. Rev. B* **99**, 224512 (2019).

[23] R. Szczęśniak, A. Barasiński, *Acta Phys. Pol. A* **116**, 1053 (2009).

[24] R. Szczęśniak, E.A. Drzazga, D. Szczęśniak, *Eur. Phys. J. B* **88**, 52 (2015).

[25] J. Bardeen, L.N. Cooper, J.R. Schrieffer, *Phys. Rev.* **106**, 162 (1957).

[26] J. Bardeen, L.N. Cooper, J.R. Schrieffer, *Phys. Rev.* **108**, 1175 (1957).